

# Adaptive Massive MIMO for fast moving connected vehicles: It will work with Predictor Antennas!

Dinh-Thuy Phan-Huy<sup>1</sup>, Stefan Wesemann<sup>2</sup>, Joachim Björnsell<sup>3</sup>, Mikael Sternad<sup>3</sup>

<sup>1</sup>Orange Labs, <sup>2</sup>Nokia Bell Labs, <sup>3</sup>Uppsala University

dinhthuy.phanhuy@orange.com, stefan.wesemann@nokia-bell-labs.com, {joachim.björnsell, mikael.sternad}@angstrom.uu.se

**Abstract**— Predicting the channel between a massive multiple input multiple output antenna and a car is a challenge, due to the short-term fading. It becomes essentially impossible by conventional extrapolation from past estimates if the car has moved by half a wavelength or more in space at the time when the channel estimate will be needed. This problem would prevent us from using the best fifth generation adaptive antenna downlink precoding schemes for very fast moving connected vehicles. A potential solution is to add another vehicle antenna, a “predictor antenna”, which senses the channel in advance. In this paper, based on drive tests and channel measurements from a 64-element antenna to a car, we for the first time show that this concept works for massive MIMO downlinks. Thanks to the use of a predictor antenna, the complex OFDM downlink channels can be predicted with an accuracy that enables maximum ratio transmit beamforming with close to ideal beamforming gain for non-line-of-sight channels. Zero forcing transmission to two users results in a signal-to-interference ratio of 20 dB to 30 dB when predicting non-line-of-sight channels up to three wavelengths ahead in space. These first experiment shows that the predictor antenna concept is a potential solution to make fifth generation adaptive antennas work for very fast moving connected vehicles.

**Keywords**—Massive MIMO, Predictor Antenna, Channel Prediction, Connected Car, 5G

## I. INTRODUCTION

Fifth generation (5G) of mobile networks will provide high capacity broadband internet service and infotainment to users on board of vehicles such as cars [1]. Because of the high in-car penetration loss, users on board of cars should not be served directly by the 5G network. Instead, they should preferably be served by a wireless access point inside the car [2]. The car itself would be connected to the 5G network via outside antennas placed upon the roof of the car [2].

Adaptive massive multiple input multiple output (M-MIMO) is a key feature of 5G [3][4]. Adaptive M-MIMO exploits a large number of antenna elements at the network side and performs downlink adaptive beamforming, either to reduce the radiated energy for a given target data rate, with maximum ratio transmission (MRT) beamforming for instance, or to increase the spectral efficiency for a given transmit power, with for instance zero forcing (ZF) beamforming.

However, M-MIMO performance is known to be very sensitive to channel aging [5][6]. Indeed, between the time when the network measures the channel  $h_p$ , and the time when the network transmits data to the car through the channel  $h_m$ , there is a time delay  $\tau$ , so the car has moved by a displacement

$\delta = v\tau$ , where  $v$  is the velocity of the car. The network uses  $h_p$  as a prediction of  $h_m$ , and computes the downlink beamforming coefficients based on this prediction. Hence,  $\tau$  is a required “prediction horizon”. In the presence of short-term fading due to multipath propagation, an estimate  $h_p$  will be an accurate prediction of  $h_m$  only under the following equivalent conditions:

$$\delta \ll \lambda,$$

$$\tau \ll \frac{c}{fv},$$

$$v \ll \frac{c}{f\tau},$$

where  $\lambda$  is the carrier wavelength,  $c$  is the speed of light and  $f$  is the carrier frequency. If these conditions are not met, then the channel is outdated. Fig. 1 illustrates the case where  $\delta = \lambda$ .

### Legend

- Current position of antenna
- Position of antenna during prediction

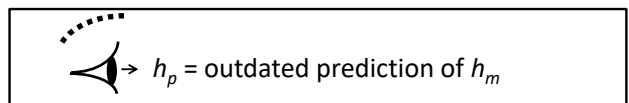
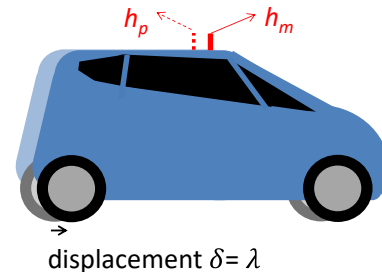


Fig. 1. Outdated channel prediction.

Experiments where adequate channel accuracy was obtained for M-MIMO channels to moving vehicles were recently reported in [19] for line-of-sight channels to moving vehicles. However, in environments with significant multi-path propagation and local scattering around the car, the impact of beamforming mis-pointing is large even for a small displacement  $\delta$  [16].

The most efficient known way to perform channel prediction for a single vehicle antenna consists of accumulating

several successive measurements (several  $h_p$ 's) and using Kalman filtering and extrapolation to predict  $h_m$  [7][8] [9][10]. Such a strategy has recently been applied to adaptive M-MIMO [11]. However, in most fading environments, it works only for limited horizons of at most half a wavelength, i.e. only for:

$$\begin{aligned} \delta &< 0.5\lambda, \\ \tau &< 0.5 \frac{c}{fv}, \\ v &< 0.5 \frac{c}{f\tau}. \end{aligned}$$

Recently, a conceptually different approach has been proposed that uses a ‘‘Predictor Antenna’’ [12][13][14][15][16]. In this approach, illustrated in Fig. 2, a ‘‘Predictor Antenna’’ is placed at the front of the ‘‘Main Antenna’’, aligned with the direction of movement of the car. In the case where the inter-antenna spacing  $d$  is larger than or equal to  $\delta$ , as illustrated in Fig. 2-a) and 2-b), the prediction can, in theory, be accurate even when  $\delta$  is close to or higher than  $\lambda$ . In general, the antenna distance  $d$  should be selected so that the longest prediction horizon in time that is required by the communication system should correspond to a movement of at most  $d$  in space, at the maximum vehicle velocity.

Legend

- | Current position of Predictor antenna
- | Position of Predictor antenna during prediction
- | Current position of antenna
- | Position of Predictor antenna during prediction

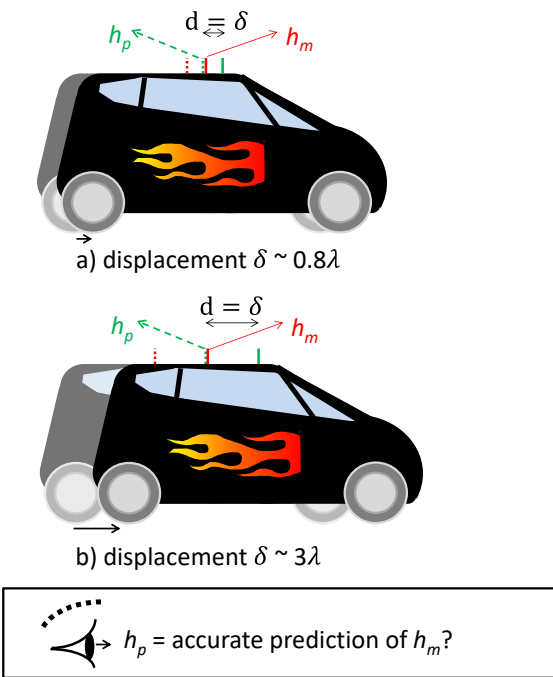


Fig. 2. Predictor Antenna that accomodates a prediction horizon that corresponds to a) a displacement  $\delta \sim 0.8\lambda$  and b) a displacement  $\delta \sim 3\lambda$ .

The accuracy of this novel prediction method has been studied using experimental measurements from drive-tests in Dresden in [12][13][14][15]. These results show that the predictor antenna provides a channel prediction that can obtain useful prediction accuracy for a prediction horizon of at least  $3\lambda$ . This is an order of magnitude longer than the horizons for which Kalman/Wiener extrapolation provides useful accuracy (typically up to  $0.3\lambda$ ). The attainable Normalized Mean Square Errors (NMSE) of predicted complex valued OFDM channel coefficients was around -10 dB in these experiments, and holds fairly constant for an increasing antenna distance  $d$ .

In [15], a real-time algorithm exploiting the Predictor Antenna is outlined and exhibits good performance. However, all these studies were so far limited to single input single output (SISO) systems. The potential use of predictor antennas has been studied in [16][17] for M-MIMO, but so far only based on simulations.

In this paper, we for the first time show that, based on experimental measurements from drive-tests, predictor antennas can provide channel predictions with useful accuracy for MRT as well as for ZF precoding. Results will be discussed for prediction horizons in space of from 0.8 wavelength (as illustrated in Fig. 2-a) up to 3 wavelengths (as illustrated in Fig. 2-b) for non-line-of-sight propagation channels.

Below, Section II describes our measurement set-up, Section III outlines the predictor antenna algorithm and the performance evaluation methodology while Section IV provides our measurement results and Section V concludes this paper.

II. MEASUREMENT SET-UP

The channel measurements were conducted on the Nokia Bell Labs campus in Stuttgart, Germany.



Fig. 3. Massive MIMO antenna of 64 antenna elements (4 lines and 16 columns of antenna elements) on the roof of a building of Nokia Bell Labs campus in Stuttgart, Germany.

At the network side, a 64-element antenna array was mounted on the roof top of a large building at a height of 20m, with a mechanical downtilt of 10 degrees. As shown in Fig. 3, the array consisted of 4 rows with 16 (dual-polarized, but only one polarization direction was used) patch antennas each, with a horizontal antenna spacing of  $\lambda/2$ , and a vertical separation of  $\lambda$ . The array transmitted an Orthogonal Frequency Division Multiplex (OFDM) waveform of around 10 MHz bandwidth at the carrier frequency of 2.180 GHz. The sub-carrier spacing was 15 kHz. In total, 600 sub-carriers spaced by 15 kHz are transmitted and 64 Time/Frequency-orthogonal pilots are used for estimating channels from all the 64 antenna elements. The pilot signals were transmitted with a periodicity of 0.5 ms.

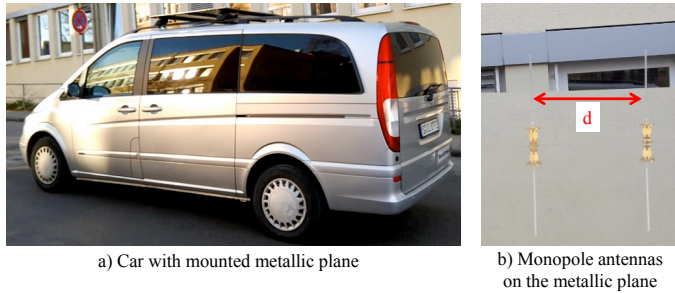


Fig. 4. Measurement vehicle setup, with antennas on the roof.

At the car side, the measurement set-up consisted of a Pendulum GPS-12R Portable unit, a Rohde & Schwarz TSMW receiver and a Rohde & Schwarz IQR hard disk recorder. As receive antenna we used two monopole antennas that are illustrated in Fig. 4-b), and positioned with distances 11 cm, 15 cm and 42 cm in different experiments. These antennas were mounted on a metallic horizontal plane installed upon the roof of the car, as illustrated in Fig. 4-a). Based on the GPS signal, the receiver was time/frequency synchronized to the transmit array and captured the received pilot signal along each route continuously over periods of 30s to 40s.

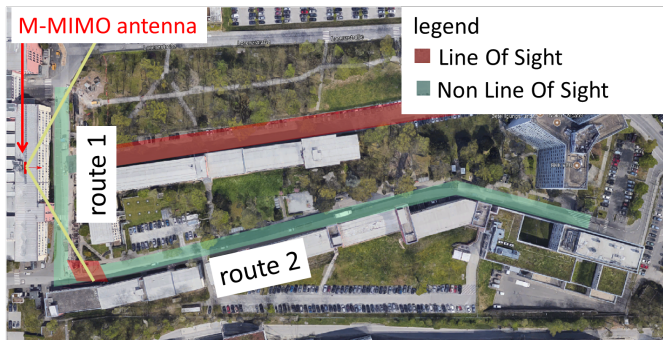


Fig. 5. M-MIMO antenna, Route 1 and Route 2.

The drive-tests that will be in focus here were made over Route 2 illustrated in Fig. 5. The position of the M-MIMO antenna is illustrated in Fig. 5 and 6. The velocity during the drive-tests was below 30 km/h, see Table 1 below.

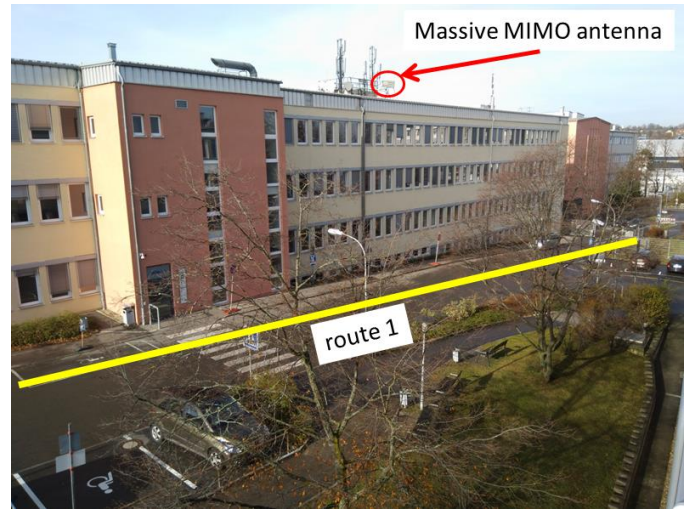


Fig. 6. M-MIMO antenna, Route 1.

During drive-tests, the channels from the 64 antenna elements of the M-MIMO to the two receive antennas of the car were measured in 50 frequency blocks of width 12 subcarriers = 180 kHz at every 0.5 ms and were stored, together with accurate time-stamps. Some subcarriers were left empty within each block of 180 kHz. These were used to measure the receiver noise power, to deduce the receive signal to noise ratio (SNR) and the noise-free received signal power.

### III. PERFORMANCE EVALUATION METHODOLOGY

#### A. Channel prediction

We here first outline the algorithm used for producing channel predictions using the prediction antenna. It is a simplified variant of the on-line scheme presented in [15]. We define:

- $N$  as the total number of time samples per drive test;
- $K = 64$  as the number of M-MIMO transmit antennas and
- $M = 50$  is the number of subcarrier frequencies spaced by 180 kHz for which the channel is measured.

We furthermore denote by  $z_{n,k,m}$  and  $z'_{n,k,m}$  the measured channel sample between transmit antenna  $k \in \llbracket 1, K \rrbracket$  and the target antenna, and between the same transmit antenna  $k$  and the predictor antenna, respectively, at time stamp  $n \in \llbracket 1, N \rrbracket$ , and for resource block  $m \in \llbracket 1, M \rrbracket$ .

For a given transmit antenna  $k$  and frequency block  $m$ , the signal propagates to the target antenna at time  $n$  over the channel  $h_{n,k,m}$ , represented by a complex scalar that includes the influence of transmit and receive processing.

The measurements on route 2 that will be studied here have a high signal-to-noise ratio (SNR) of around 30 dB, and the resulting channel estimate-to estimation error power ratio also becomes around 30 dB. We will therefore in the following assume that the measured channels to the target antenna represent the actual channels:

$$h_{n,k,m} = z_{n,k,m}.$$

Likewise, the estimated channels to the predictor antenna  $z'_{n,k,m}$  are accurate, and will here be used directly. In general, in environments with lower SNR, filtering or smoothing should be applied to the channel measurements for predictor antennas to suppress estimation errors, as discussed in [14] and [15].

The prediction of the channel to the target antenna for a prediction horizon  $\tau$  timesteps ahead can now be obtained in a very simple way;

$$h_{n+\tau,k,m}^{\text{pred}} = a_{k,m} z'_{n+\tau-g,k,m}. \quad (1)$$

Here,  $a_{k,m}$  is a complex-valued scalar gain used at subcarrier  $m$  for downlink channel  $k$ . In a stationary fading environment, its Mean Square Error (MSE)-optimal value can be shown to be

$$a_{k,m}^{\text{opt}} = \frac{\mathbb{E} |z_{n,k,m} (z'_{n-g,k,m})^*|}{\sigma_{k,m}^2}, \quad (2)$$

where  $*$  denotes complex conjugate, the average is with respect to the short-term fading statistics and where  $\sigma_{k,m}^2$  is the average power of the measured predictor antenna channel  $z'_{n,k,m}$ . The ideal case, with normalized correlation  $a_{k,m}^{\text{opt}} = 1$ , implies perfect predictability [12],[14].

The delay  $g=d/v$  in (1) and (2) represents the time it takes for the vehicle to travel the distance  $d$  between the two antennas at velocity  $v$ . Predictions for horizons  $\tau \leq g$  can then be produced by (1) by interpolating between the latest and the previously obtained channel estimates for the predictor antenna. In our investigations below, we restrict the focus to prediction horizons in time that equal the delay due to the antenna distance in space,  $\tau = g$ .

The delay  $g$  can be estimated without relying on external estimates of the vehicle velocity  $v$ . We estimate it as the delay  $l$  that maximizes the amplitude of the cross correlation  $c_{l,k,m}$  between main antenna channel and the predictor antenna channel and we use the median over subcarriers  $m$  and downlink channels  $k$ , which is robust to outliers in the statistics. The expressions of  $c_{l,k,m}$  and the estimated delay  $\hat{g}$  are given by:

$$c_{l,k,m} = \frac{1}{N_1} \sum_{n=N_0}^{N_0+N_1} z_{n,k,m} (z'_{n-l,k,m})^* \text{ and} \quad (3)$$

$$\hat{g} = \text{Median}_{k,m} \left( \arg \max_l |c_{l,k,m}| \right). \quad (4)$$

The correlations are measured over a time interval over which the velocity can be considered approximately constant. We use length  $N_1 - N_0 = 1000$ , corresponding to 0.5 s. Using the power estimate

$$\hat{\sigma}_{k,m}^2 = \frac{1}{N_1} \sum_{n=N_0}^{N_0+N_1} |z'_{n,k,m}|^2 \quad (5)$$

and the estimated maximal correlation (3), the estimated prediction coefficient to be used in (1) becomes

$$a_{k,m} = \frac{c_{\hat{g},k,m}}{\hat{\sigma}_{k,m}^2}. \quad (6)$$

The prediction coefficients  $a_{k,m}$  are adjusted for all downlink channels  $k$  and subcarriers  $m$  separately. The adjustment described above takes e.g different gains and phase shifts induced by the receivers of the target antenna and the predictor antenna into account.

We will at the end of Section IV study the impact of using an even simpler predictor scheme that sets

$$a_{k,m} = 1 \quad (7)$$

in (1). This non-optimal choice would induce an amplitude error (since the normalized correlation (2) in general has amplitude below 1) and also a phase error. However, the channel predictions produced by such a ‘‘trivial’’ predictor antenna scheme will turn out to be useful for maximum ratio transmit beamforming. We also apply a random error to  $\tau$ ,  $|g - \tau| < 5T$ , where  $T = 0.5$  ms.

### B. MRT performance evaluation metric: the normalised received power

When MRT is applied in the downlink and is based on the predicted channels (1), the received power averaged over subcarriers, becomes

$$r(n) = \frac{1}{M} \sum_{m=1}^M \left| \sum_{k=1}^K h_{n,k,m} \left( \frac{h_{n,k,m}^{\text{pred}}}{\alpha_n^{\text{pred}}} \right)^* \right|^2, \quad (8)$$

when using a normalization  $\alpha_n^{\text{pred}}$  such that the total transmit power is 1, i.e.:

$$\sum_{k=1}^K \sum_{m=1}^M \left| \frac{h_{n,k,m}^{\text{pred}}}{\alpha_n^{\text{pred}}} \right|^2 = 1. \quad (9)$$

We furthermore define  $r_{\text{ideal}}(n)$  as the received power  $r(n)$  attained with ideal prediction  $h_{n,k,m}^{\text{pred}} = h_{n,k,m}$ , and define the normalized received power  $r_{\text{norm}}(n) \in [0,1]$  as:

$$r_{\text{norm}}(n) = r(n) / r_{\text{ideal}}(n). \quad (10)$$

### C. ZF performance evaluation metric: Signal-to-Interference Ratio

For ZF, we here evaluate a case with two spatially multiplexed users. The measured channels are used as channels to the first user. We then create channels for a second simultaneous ‘‘imaginary user’’ that is to be spatially multiplexed with the first user. The channels for this imaginary user are created by taking the measured ones, i.e. the ones for the first user and cyclically shifting them in the frequency domain. This generates a set of channels that has similar properties as the current measured channel, in both the frequency and spatial domain, but that is also different from these first user channels and likely to be un-correlated.

Specifically, we create the MIMO channel matrix  $\mathbf{H}^{(n,m)} \in \mathbb{C}^{2 \times K}$  with rows  $\mathbf{H}_{l,k}^{(n,m)} \in \mathbb{C}^{1 \times K}$ , describing the channels to the two users (indexed by  $l = 1,2$ ) as follows:

$$\mathbf{H}_{1,k}^{(n,m)} = h_{n,k,m}, \quad (11)$$

$$\mathbf{H}_{2,k}^{(n,m)} = h_{n,k,n,k,[(m+23) \bmod M]+1}.$$

We also create the corresponding predicted MIMO channel matrix  $\mathbf{H}^{(n,m,\text{pred})} \in \mathbb{C}^{2 \times K}$  with rows  $\mathbf{H}_{l,k}^{(n,m,\text{pred})} \in \mathbb{C}^{1 \times K}$  as

$$\mathbf{H}_{1,k}^{(n,m,\text{pred})} = h_{n,k,m}^{\text{pred}} \quad (12)$$

$$\mathbf{H}_{2,k}^{(n,m,\text{pred})} = h_{n,k,[(m+23) \bmod M]+1}^{\text{pred}}.$$

We then define the corresponding ZF precoder  $\mathbf{P}^{(n,m)} \in \mathbb{C}^{K \times 2}$  that is based on the predicted channel vectors

$$\mathbf{P}^{(n,m)} = (\mathbf{H}^{(n,m,\text{pred})})^\dagger \left( \mathbf{H}^{(n,m,\text{pred})} (\mathbf{H}^{(n,m,\text{pred})})^\dagger \right)^{-1}, \quad (13)$$

where  $(\cdot)^\dagger$  denotes Hermitian transpose. When applying this precoder, the users will then receive their data through the equivalent MIMO channel matrix  $\mathbf{G}^{(n,m)} \in \mathbb{C}^{2 \times 2}$

$$\mathbf{G}^{(n,m)} = \mathbf{H}^{(n,m)} \mathbf{P}^{(n,m)}. \quad (14)$$

The resulting signal to interference ratio (SIR) experienced due to interference from the other user is here measured as an average over the two users:

$$\text{SIR}(n,m) = \frac{1}{2} \left( \frac{|\mathbf{g}_{1,1}^{(n,m)}|^2}{|\mathbf{g}_{1,2}^{(n,m)}|^2} + \frac{|\mathbf{g}_{2,2}^{(n,m)}|^2}{|\mathbf{g}_{2,1}^{(n,m)}|^2} \right). \quad (15)$$

#### IV. RESULTS

In our study, the channel sampling rate is  $T = 0.5$  ms, the number of recorded channel samples  $N$  depends on the drive-test,  $K = 64$  and  $M = 50$ . The evaluated drive-tests differ by the direction of driving and by the inter-antenna spacing  $d$  as shown in Table I.

TABLE I. DRIVE-TESTS

N°	Parameters		
	Direction on Route 2	Velocity (km/h)	$d$ (cm)
1	West to East	15	11
2	East to West	25	11
3	West to East	25	42
4	West to East	15	15

##### A. Results for MRT beamforming

The result of MRT beamforming is now evaluated by simulation, using the measured and the predicted channels for the target antenna. Fig. 7 shows cumulative distribution functions (Cdfs) over all time samples and all subcarriers of the normalized received power  $r_{\text{norm}}(n)$  defined by (10), for the four test routes. The results are compared to those obtained when using outdated channels to the target antenna instead, i.e. when using

$$h_{n+\tau,k,m}^{\text{outdated}} = z_{n,k,m} \quad (16)$$

instead of (1). It is evident from Figure 7 that use of outdated channels results in a significant beamforming power loss, while the use of the predictor (1) provides channel gains within less than 1 dB of the maximal attainable gains.

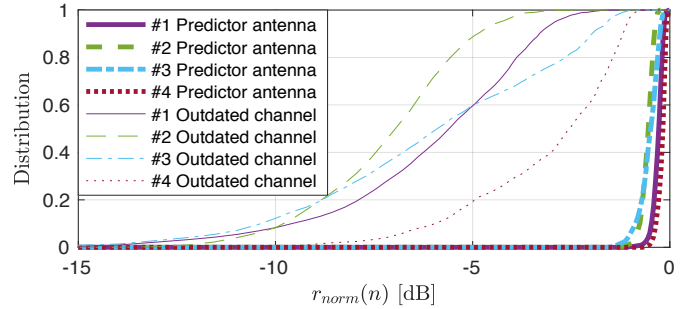


Fig. 7. Cdfs of normalized received beamformed power by (10), when using MRT beamforming, based on channel predictions from predictor antennas, for outdated channel predictions, and ideal prediction, in the four drive tests of Table I. The utilized prediction horizons in space equal the antenna distance, which differs between the cases, see Table I.

To illustrate the time-evolution of the received power and the normalized received power, Fig. 8 and Fig. 9 show the time-evolutions of these quantities for Drive-Test number 1 and Drive-Test number 3, respectively. The right-hand figures show the normalized beam power gains  $r_{\text{norm}}(n)$  by (10). The left-hand figures show the received power with ideal prediction, normalized by the average received power over the whole route, defined by

$$R_{\text{ideal}}(n) = r_{\text{ideal}}(n) / \sigma_{r_{\text{ideal}}}, \quad (17)$$

where  $\sigma_{r_{\text{ideal}}}^2 = \frac{1}{N} \sum_{n=1}^N |r_{\text{ideal}}(n)|^2$ .

In the Drive-Test 1 illustrated by Figure 8, the antenna distance is 11 cm or 0.8 wavelengths and the corresponding prediction horizon in time that we evaluate here at 15 km/h = 4.2 m/s is then 26 ms. The receive power decreases with time. This does not appreciatively affect the normalized received power after beamforming, which stays close to the ideal value at all measurements along the route.

In the Drive 3 illustrated in Figure 9, the antenna distance is 42 cm, or close to 3 carrier wavelengths. We use a correspondingly long prediction horizon which at 25 km/h = 7 m/s is 60 ms. During the first half of this drive, where the received power is high, beamforming that uses the outdated channel performs quite well. This is likely due to the channel being dominated by one very strong reflex, which reduces the relative influence of multipath fading. During the second half of the drive, between time 1.5 s and 3.0 s, use of the outdated channels performs poorly, while the MRT beamformers based on the predictor antenna estimates perform close to ideal, despite the use of a very long prediction horizon.

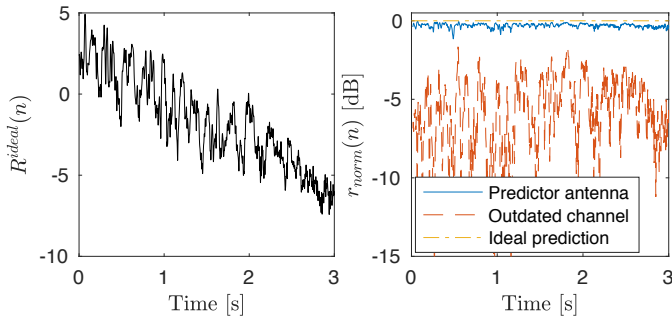


Fig. 8. Time evolution of received ideal beamformed power by (17) (left) and the normalized received power by (10) (right), in Drive-Test 1.

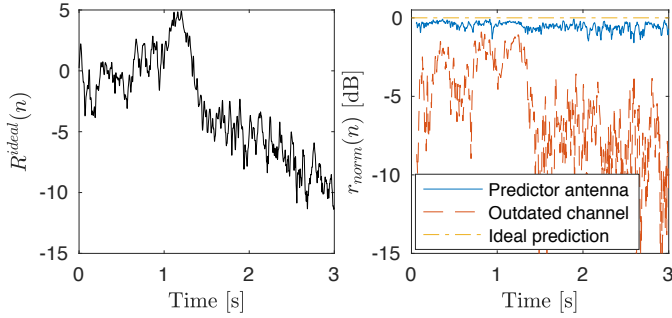


Fig. 9. Time evolution of received ideal beamformed power by (17) (left) and the normalized received power by (10) (right), in Drive-Test 3.

### B. Results for ZF beamforming

The result of ZF precoding is now evaluated by simulation, using the measured and the predicted channels for the target antenna. Figure 10 shows cumulative distribution functions over all time samples and subcarriers of the average SIR of the two users, by (15), for the four test routes. The results are compared to those obtained when using outdated channels (16). The use of predictor antennas improves the SIR from typically around 5-15 dB to mostly between 20-30 dB, with Drive 3 giving a somewhat worse performance than the other cases. This is the case with the longest antenna distance.

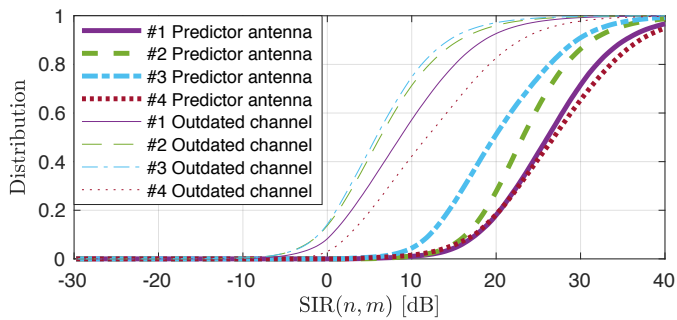


Fig. 10. Distributions of the average SIRs of two users by (15), when using ZF transmit beamforming, with use of predictor antennas and for outdated channel predictions, in the four drive tests of Table 1. The utilized prediction horizons in space equal the antenna distance, which differs between the cases.

In Figure 11 we exemplify the time-evolutions of the SINRs, averaged over subcarriers in logarithmic scale. In this and in the other three drive tests, there is a significant gap

between the SIR performance with outdated channels and the performance with prediction antennas at all times along the routes.

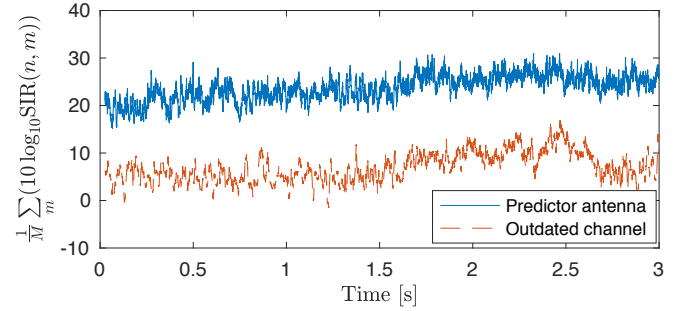


Fig. 11. The residual SIR, averaged for the two users and averaged over all subcarriers, along Drive 2, when applying zero forcing transmit beamforming using channels estimates from predictor antennas and outdated channel estimates.

### C. Robustness of the MRC beamforming gain

Fig. 12 shows the performance loss when using the extremely simple predictor by (7) instead of (1). We have here also introduced a rectangular distributed error in the estimate of the correlation peak lag  $g$  (or, equivalently, to the prediction horizon  $\tau$ ) with a rectangular spread of  $\Delta g = \pm 5$  time steps  $T$ , or 2.5 ms.

Use of the simple predictor coefficient (7) will definitely not generate good predictions of the complex channels to the target antenna. It produces large prediction errors on average. However, when MRT beamforming is used, as exemplified for Drive-Test number 1 in Fig. 12, the resulting reduction of the attained beamforming gains, as compared to the use of (6) in (1), becomes remarkably low.

There are two main explanations for this. First, the phase and amplitude errors caused by using  $a_{k,m} = 1$  instead of (6) are mainly systematic over different antenna channels  $k$ . Such common phase errors will not affect the resulting MRC beamforming gain (8), and common amplitude errors are canceled by the transmit power normalization (9).

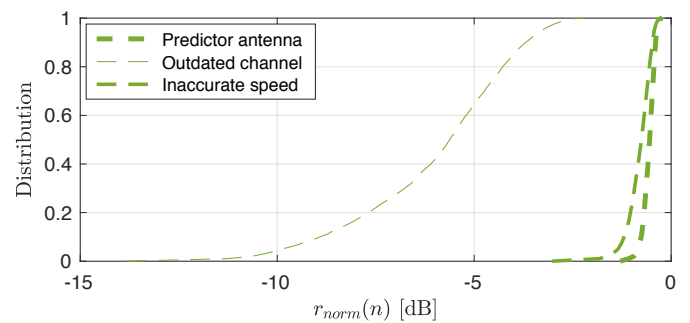


Fig. 12. Cdfs of normalized received beamformed power by (10), when using MRT beamforming, based on channel predictions from predictor antennas with simple processing (7) and inaccurate speed estimates, with accurate processing (1), and with outdated channel predictions, for Drive-Test 1.

A second explanation is that MRT beamforming is robust to slight mispointing. For example, a timing lag error  $|\tau - g| < T$  seconds will correspond to a residual mispointing (in the spatial domain) of  $vT = 0.015$  wavelengths (at  $v = 15$  km/h and  $T = 0.5$  ms). In a Rayleigh fading channel with uniform angular spread of paths for instance, the result of MRT beamforming, as for the transmit matched filter or Time Reversal pre-filter, would result in a normalized power  $J_0\left(2\pi\frac{vT}{\lambda}\right) = 0.9999$ , where  $J_0(\cdot)$  is the zero<sup>th</sup>-order Bessel function of the first kind [20].

#### D. Consequences for predictability at high velocities

We have here illustrated that very long prediction horizons can be handled at the relatively slow vehicle speeds at which the drive tests were obtained. These results can be transformed to results at higher velocities using the relation  $d = \delta = v\tau$ .

For example, if we consider in practice, a delay between measurement and beamforming of  $\tau = 5$  ms, then the maximum velocity for which M-MIMO MRT is supportable by a predictor antenna system with 42 cm distance between antennas is given by:

$$v = \frac{d}{\tau} = \frac{0.42}{0.005} = 302 \text{ km/h.}$$

With a latency of only  $\tau = 3$  ms, this speed limit for the M-MIMO MRT to work is adequate for high speed trains:

$$v = \frac{d}{\tau} = \frac{0.42}{0.003} = 503 \text{ km/h.}$$

It should be noted that antenna distances of 3 wavelengths are by no means a limit for prediction antenna systems, this is only the longest separation that we have evaluated so far.

It should however also be noted that to obtain channel estimates at these very high velocities, the pilot transmission must occur at sufficiently high frequency with respect to the fading, i.e. at least twice the maximal Doppler frequency at the corresponding velocity. This is not a limitation imposed by the predictor antenna system but a fundamental limitation that has consequences for standardization. With sparse sampling of the fading channel, it also becomes important to use a good scheme for interpolating between predictor antenna channel estimates to obtain the predicted channel at the precise required position in space that corresponds to the prediction horizon  $\tau$ . This issue is under current investigation.

#### V. CONCLUSIONS

Predicting the channel between a massive MIMO antenna and a car that moves by one wavelength or more is a challenge. For the first time, drive tests with measurements from a 64-element massive MIMO antenna show that the complex OFDM downlink channels can be predicted with an accuracy that enables maximum ratio transmit beamforming with close to ideal beamforming gain for non-line-of-sight channels. We have also shown that Zero forcing transmission to two users can result in average signal-to-interference ratios of 20 dB to 30 dB when predicting non-line-of sight channels up to three wavelengths ahead in space. The attained accuracy is much higher than when using outdated channel estimates.

Our continued studies will focus on running and evaluating a real-time prediction algorithm based on the Predictor Antenna concept, assuming a realistic time-frame structures in TDD systems. We also intend to further evaluate the hardware, software and system design factors that affect the performance of a predictor antenna system.

#### ACKNOWLEDGMENT

The authors would like to thank Prof. A. Pascht for initiating this cooperation between Orange and Nokia. They are also grateful for the support from G. Kaltbeitzel, D. Wiegner, M. Kinzler, S. Merk and S. Woerner. This work has been partially performed in the framework of the H2020 project 5GCAR co-funded by the EU. The views expressed are those of the authors and do not necessarily represent the project. The consortium is not liable for any use that may be made of any of the information contained therein. The Uppsala University contribution is partly funded by Orange Contract H1221.

#### REFERENCES

- [1] "5G Automotive vision" A. Kwoczek et. al. 5G Partnership Project White Paper, Oct. 2015. <https://5g-ppp.eu/wpcontent/uploads/2014/02/5G-PPP-White-Paper-on-Automotive-Vertical-Sectors.pdf>
- [2] Y. Sui, J. Vihriälä, A. Papadogiannis, M. Sternad, W. Yang and T. Svensson, "Moving cells: A promising solution to boost performance for vehicular users," *IEEE Comm. Mag.*, vol. 51, no. 6, June 2013, pp. 62-68.
- [3] F. Rusek, D. Persson, B.K. Lau, E.G. Larsson, T.L. Marzetta, O. Edfors and F. Tufvasson, "Scaling up MIMO: Opportunities and challenges with very large arrays," *IEEE Signal Processing Magazine*, vol. 30, no. 1, Jan. 2013.
- [4] V. Jungnickel, K. Manolakis, W. Zirwas, B. Panzner, V. Braun., M. Lossow, M. Sternad, R. Apelfröjd and T. Svensson, "The role of small cells, coordinated multipoint, and massive MIMO in 5G," *IEEE Comm. Magazine*, vol.52, no.5, pp.44-51, May 2014.
- [5] K. T. Truong and R. W. Heath Jr., "Effects of channel aging in massive MIMO systems," *J. Commun. and Networks*, vol. 15, no. 4, pp. 338-351, Aug. 2013.
- [6] D.-T. Phan-Huy and M. H elard, "Large MISO beamforming for high speed vehicles using separate receive & training antennas," *IEEE Int. Symposium on Wireless Vehicular Communication*, June 2013.
- [7] D. Aronsson, Channel Estimation and Prediction for MIMO OFDM Systems - Key Design and Performance Aspects of Kalman-based Algorithms. Ph.D. Thesis, Signals and Systems, Uppsala University, March 2011. [www.signal.uu.se/Publications/pdf/a112.pdf](http://www.signal.uu.se/Publications/pdf/a112.pdf)
- [8] T. Ekman, A. Ahl en and M. Sternad, "Unbiased power prediction on Rayleigh fading channels," *IEEE Vehicular Technology Conference VTC2002-Fall*, Vancouver, Canada, Sept. 2002.
- [9] T. Ekman, Prediction of Mobile Radio Channels: Modeling and Design. Ph.D. Thesis, Signals and Systems, Uppsala Univ., 2002. Available: [www.signal.uu.se/Publications/pdf/a023.pdf](http://www.signal.uu.se/Publications/pdf/a023.pdf)
- [10] A. Duel-Hallen, "Fading channel prediction for mobile radio adaptive transmission systems," *Proc. of the IEEE*, vol. 95, no. 12, pp. 2299-2313, Dec. 2007.
- [11] S. Kashyap, C. Moll en, E. Bj ornson and E. G. Larsson, "Performance analysis of (TDD) massive MIMO with Kalman channel prediction," *2017 IEEE International Conference on Acoustics, Speech and Signal Processing (ICASSP)*, New Orleans, LA, 2017, pp. 3554-3558.
- [12] M. Sternad, M. Grieger, R. Apelfr ojd, T. Svensson, D. Aronsson and A. Belen Martinez, "Using "predictor antennas" for long-range prediction of fast fading moving relays," *IEEE Wireless Communications and Networking Conference (WCNC)*, Paris, April 2012.

- [13] N. Jamaly, R. Apelfröjd, A. Belen Martinez, M. Grieger, T. Svensson, M. Sternad and G. Fettweis, "Analysis and measurement of multiple antenna systems for fading channel prediction in moving relays," *European Conference on Antennas and Propagation, (EuCAP 2014)*, April 6-11 2014, Hauge, The Netherlands.
- [14] J. Björnsell, M. Sternad and M. Grieger, "Using predictor antennas for the prediction of small-scale fading provides an order-of-magnitude improvement of prediction horizons," *2017 IEEE International Conference on Communications Workshops (ICC Workshops)*, Paris, June 2017, pp. 54-60.
- [15] J. Björnsell, M. Sternad and M. Grieger, "Predictor Antennas in Action," *2017 IEEE PIMRC*, Montreal, October 2017.
- [16] D-T Phan-Huy, M. Sternad and T. Svensson, "Making 5G adaptive antennas work for very fast moving vehicles," *IEEE Intelligent Transportation Systems Magazine*, Summer, 2015, pp. 71-84.
- [17] D.-T. Phan-Huy, M. Sternad, T. Svensson, W. Zirwas, B. Villeforceix, F. Karim and S.-E. El-Ayoubi, "5G on board: How many antennas do we need on connected cars?" *IEEE Globecom 2016 Workshop on 5G RAN Design*, Washington DC, Dec. 2016.
- [18] E. Björnsson, J. Hoydis, M. Kountouris and M. Debbah, "Massive MIMO systems with non-ideal hardware: Energy efficiency, estimation, and capacity limits," *IEEE Trans. on Information Theory*, vol. 60, no. 11, pp. 7112-7139, Nov. 2014.
- [19] P. Harris, S. Malkowsly, J. Vieira, E. Bengtsson, F. Tufvesson, W. Boukley Hasan, L. Liu, M. Beach, S. Armour and O. Edfors, "Performance characterization of a real-time massive MIMO system with LOS mobile channels," *IEEE Journal on Selected Areas in Communications*, vol. 35, no. 6, June 2017, pp. 1244-1253.
- [20] V. D'Amico et al. Deliverable D1.2 "Innovative advanced signal processing algorithms for interference avoidance", section 4.1.3, Artist 4G Project, available at: [http://publications.lib.chalmers.se/records/fulltext/134553/local\\_134553.pdf](http://publications.lib.chalmers.se/records/fulltext/134553/local_134553.pdf)